NASA Contractor Report 198469

Soot Precursor Material: Spatial Location via Simultaneous LIF-LII Imaging and Characterization via TEM

Randall L. Vander Wal
NYMA, Inc.
Brook Park, Ohio

May 1996

Prepared for
Lewis Research Center
Under Contract NAS3–27186

National Aeronautics and
Space Administration

Soot Precursor Material: Spatial Location via Simultaneous LIF-LII imaging and Characterization via TEM

Randall L. Vander Wal*
NYMA@ NASA-Lewis
Cleveland, OH 44135

Abstract
The chemical and physical transformation between gaseous fuel pyrolysis products and solid carbonaceous soot represents a critical step in soot formation. In this paper, simultaneous two-dimensional LIF-LII images identify the spatial location where the earliest identifiable chemical and physical transformation of material towards solid carbonaceous soot occurs along the axial streamline in a normal diffusion flame. The identification of the individual LIF and LII signals is achieved by examining both the excitation wavelength dependence and characteristic temporal decay of each signal. Spatially precise thermophoretic sampling measurements are guided by the LIF-LII images with characterization of the sampled material accomplished via both bright and dark field TEM. Both bright and dark field TEM measurements support the observed changes in photophysical properties which account for conversion of fluorescence to incandescence as fuel pyrolysis products evolve towards solid carbonaceous soot.

Introduction

Among the intermediate combustion species, polycyclic aromatic hydrocarbons (PAHs) have been identified as a necessary chemical precursor species for soot formation within both premixed and diffusion flames. Through both physical and/or chemical condensation, large PAHs form soot precursor particles [1-4]. These particles have been identified by transmission electron microscopy (TEM) of thermophoretically sampled material from both a low pressure premixed acetylene/oxygen flame [1] and recently diffusion flames [5,6]. Yet the process(es) by which condensed PAHs transform into soot are not well understood.

Specific Objectives

Given the critical link that soot precursor material provides between molecular fuel pyrolysis products such as PAHs and carbonaceous soot, characterization of the hemical/physical transformation process is essential in understanding soot formation [7]. Since the axial streamline of a gas-jet diffusion flame mirrors a 1-d flow system, (no radial velocity component) the temporal evolution of the material transformation within the same gas volume element can be observed at different axial heights. Recently, simultaneous LIF-LII images have been obtained in a gas-jet diffusion flames clearly defining the fuel pyrolysis (via LIF) and soot containing (via LII) regions [6]. Moreover, the LIF-LII images demarcated the spatial region where a material transformation of gaseous fuel pyrolysis products towards solid carbonaceous soot began. These prior measurements were performed within a low Reynolds number (Re = 17, calculated for cold gas flow) flame in an effort to minimize buoyant acceleration of the flow. TEM of thermophoretically sampled material confirmed the presence of soot precursor particles within this region. The generality of the combined LIF-LII technique is tested here within a fully-developed laminar diffusion flame along the axial centerline which offers a longer integrated temperature-time history in which to follow this transformation.

Experimental

Light at either 1064 nm or 266 nm was used for LII and combined LIF-LII measurements respectively. An 8x Galilean telescope of spherical UV fused silica lenses followed by a pair of cylindrical lenses and aperture formed a 20 mm high laser sheet. Typical intensities for the 1064 nm light in the sheet were estimated to be 3×10^7 W/cm^2 based on a 10 ns laser pulse and sheet thickness of 750 microns. Using a 5 ns pulse width (FWHM) and 500 micron sheet thickness for the 266 nm light yielded an approximate intensity of 1×10^6 W/cm^2. For two-dimensional images, a gated intensified camera fitted with an ultraviolet f4.5/ 105mm (adjustable) focal length camera lens and 40 mm extension tube captured the LII and simultaneous LIF-LII images. A bandpass filter (400 to 450 nm) preceded the gated intensified array camera for both the LII and simultaneous LIF-LII measurements. A frame-grabber digitized the images for transfer to the host computer.

The burner consisted of a fuel nozzle of 11.1 mm outer diameter surrounded by a 101 mm diameter ceramic honeycomb used to provide a laminar air coflow [8]. Ethylene flow rates of 0.231 slpm and air flow rate of 42.8 slpm were used. An air-actuated piston driving a rod holding the TEM grid holder and grid was used for thermophoretic sampling measurements.

*Corresponding author
Proceedings of the 1996 Technical Meeting of the Central States Section of the Combustion Institute.

Results and Discussion

LIF-LII Images

To identify the origin of the signals induced by each excitation wavelength, spatially resolved measurements are required. Both the excitation wavelength dependence and temporal behavior identify the origin of the LIF-LII signals from the region centered at 30 mm HAB [11]. Figures 1(a) to 1(c) illustrate LIF-LII images obtained using 266 nm excitation light while Figs. 1(d) to 1(f) reveal two-dimensional LII images of the same spatial region using 1064 nm excitation.

Light at 266 nm is known to readily excite electronic transitions in a variety of combustion intermediates and also create electronically excited photofragments resulting in often undesirable fluorescence [9,10]. In contrast, 1064 nm light is not absorbed by molecular combustion intermediates. To excite fluorescence, multiphoton absorption of 1064 nm light is necessary. Not only is nonresonant multiphoton absorption unlikely at these laser intensities, but even if it did occur would likely result in molecular fragmentation from the ground electronic state [11]. Such fragmentation does not lead to electronically excited photofragments capable

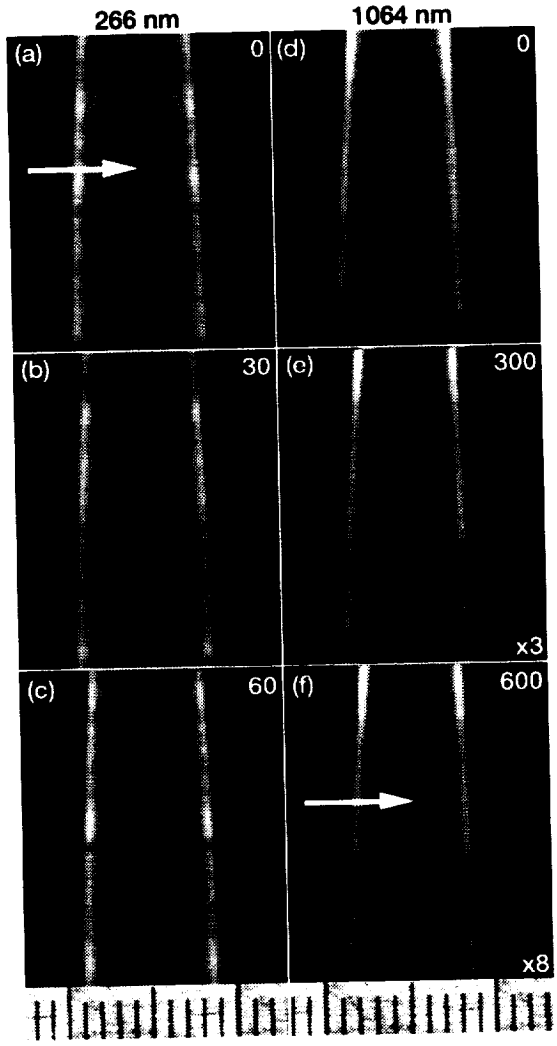

Figure 1.—Spatially resolved laser-induced emission images using either 266 nm (a-c) or 1064 nm light (d-f). The numbers in the upper right hand corner indicate the time delay between the excitation laser pulse and the leading edge of the intensifier gate pulse of 100 nsec duration. A bandpass interference filter transmitting 400-450 nm was used for each set of images. Each image is the average of 10 single laser-shot images. The ruler spatial scale is in millimeters. The arrows in panels (a) and (f) marks the transition region in which a fundamental change in the photophysical properties occurs and where thermophoretic sampling measurements were performed for subsequent TEM analysis. Neutral density filters were used to maintain LII and LIF-LII images within approximately the same signal level for a fixed camera gain. The relative intensity differences between the images resulting from this procedure are given where appropriate in the lower right hand corner of individual panels.

of fluorescence. Thus the absence of signal in the lower axial region in Figs. 1(d) to 1(f) obtained using 1064 nm light while its occurrence in Figs. 1(a) to 1(b) using 266 nm light suggests that the laser-induced emission signal in the lower axial region is not soot incandescence but rather molecular fluorescence. The rapid temporal decay of the laser-induced emission signal near the axial region shown in Figs. 1(a) to 1(c) confirms the identity of this signal as fluorescence since even in the absence of oxygen, collisional quenching within atmospheric pressure flames results in fluorescence lifetimes of tens of nanoseconds [6,12].

Since light at 1064 and 266 nm is readily absorbed by soot, at sufficient intensities both wavelengths are capable of producing LII. The similar spatial extent of the laser-induced emission signal in the annular and upper axial region using either 1064 or 266 nm light shown in Fig. 1 suggests that this signal is LII. Since cooling processes, which determine the temporal decay of the LII signal [13-16] are far slower than collisional quenching of fluorescence [16], LII is detectable hundreds of nanoseconds after the laser pulse [17-19]. Thus, the long temporal decay of the laser-induced emission signal in the annular and upper axial region extending hundreds of nanoseconds using 1064 nm excitation light (Figs. 1(d) to 1(f)) in contrast to tens of nanoseconds for the fluorescence using 266 nm light, (Figs. 1(a) to 1(c)) confirms the identity of this signal as LII. Since the axial streamline allows following the chemical/physical transformation of the same gas-volume element from fuel pyrolysis products towards solid carbonaceous soot, further discussion of the LIF and LII signals focuses upon the spatial variation of the LIF and LII signals along the axial centerline of the flame.

Interpretation of LIF-LII Origins

As seen in Figs. 1(a) to 1(c), the fluorescence intensity decreases with increasing axial height. Although increased temperature can decrease the fluorescence quantum yield, since it varies little along the the centerline near 30 mm HAB [20], the fluorescence intensity decrease is likely caused by other factors. Specifically, the decrease in the fluorscence intensity is likely due to a decrease in the gas-phase PAH concentrations. Large PAHs presumably serve as 'building blocks' for soot precursor particles while small PAHs serve as initial mass growth material for the precursor particles [2,3,21].

While fluorescence from pyrolysis regions within flames has widely been attributed to gas-phase PAH fluorescence, soot precursor particles may also fluoresce since the constituent "molecules" possess highly absorbing chromophoric groups. High molecular mass material sampled from the pyrolysis region of slightly sooting premixed flames has exhibited fluorescence upon ultraviolet excitation [22]. However, as carbonization continues, the "molecules" lose their individual identity and assimilate into an object more solid in form. With increasing solid structure, the probability for nonradiative decay dramatically increases due to the much higher quantum state density [23]. While the particles readily absorb light, with increasing carbonization, the fluorescence quantum yield from the soot precursor material decreases relative to isolated gas-phase molecules and eventually becomes negligible.

With increasing solid-state character, energy deposited in the particle through multiphoton absorption is rapidly dissipated internally [24]. Absorption at ever increasingly longer wavelengths also becomes possible. If a sufficient number of photons are absorbed, the particle will be heated to incandescence temperatures irregardless of excitation wavelength. The attainment of sufficient carbonization to yield a solid structure capable of LII is seen in the upper axial regions in Figs. 1(d) to 1(f). Following the axial streamline, beyond a certain axial height, an elemental gas volume has experienced a sufficiently long integrated temperature-time trajectory to yield carbonaceous soot. Undoubtedly, the carbonization process is far from complete. The axial height at which LII signal becomes detectable increases with increasing temporal delay between the excitation laser pulse and camera detection gate. This is shown in Figs. 1(d) to 1(f) and suggests that carbonization of the soot precursor material continues with increasing integrated temperature-time history. Although a range of particle properties, at each axial height (residence time), is suggested by the spatially overlapping LII and LIF signals along the axial centerline as seen by comparing Figs. 1(a) and 1(f), the decreasing LIF signal and the emerging LII signal along a well defined streamline demarcates a fundamental change in the material photophysical properties. Thus, the necessary change in the material physical structure from gas-phase molecular species to solid carbonaceous soot appears to be paralled by a concurrent change in the photophysical properties of the material.

Material Characterization

Observations and Interpretations

Figures 2(a) and 2(c) are bright field TEM images of soot precursor material collected 30 mm HAB as indicated by the arrow in Fig. 1(a). Figures 2(b) and 2(d) are corresponding dark field TEM images of the respective bright field images. Figures 2(e) and 2(f) show corresponding bright and dark field images of a "normal" appearing soot aggregate obtained from the annular region at this height for comparison.

The wide variation of particle sizes, shapes and opacities observed within Figs. 2(a) and 2(c) were typical of several thermophoretic samples. Samples obtained from the annular region showed a dominance of normal appearing soot aggregates such as shown in Fig. 2(e). Although the more opaque and geometrically well defined particles (Figs. 2(a) and 2(c)) could be the result of "pickup" during the probe insertion and extraction process, these particles are more likely present within the axial region along with the translucent globules. The clear geometric definition of the more opaque objects shown in Figs. 2(a) and 2(c) clearly indicate that the diffuse indistinct appearance of neighboring particles is not due to focussing. The transparency of the globules relative to the "normal" appearing soot aggregate (as shown in Fig. 2(e)) shown is attributed to lower material density. The globular shape with poor geometric definition suggests a rather fluid physical state at flame temperatures

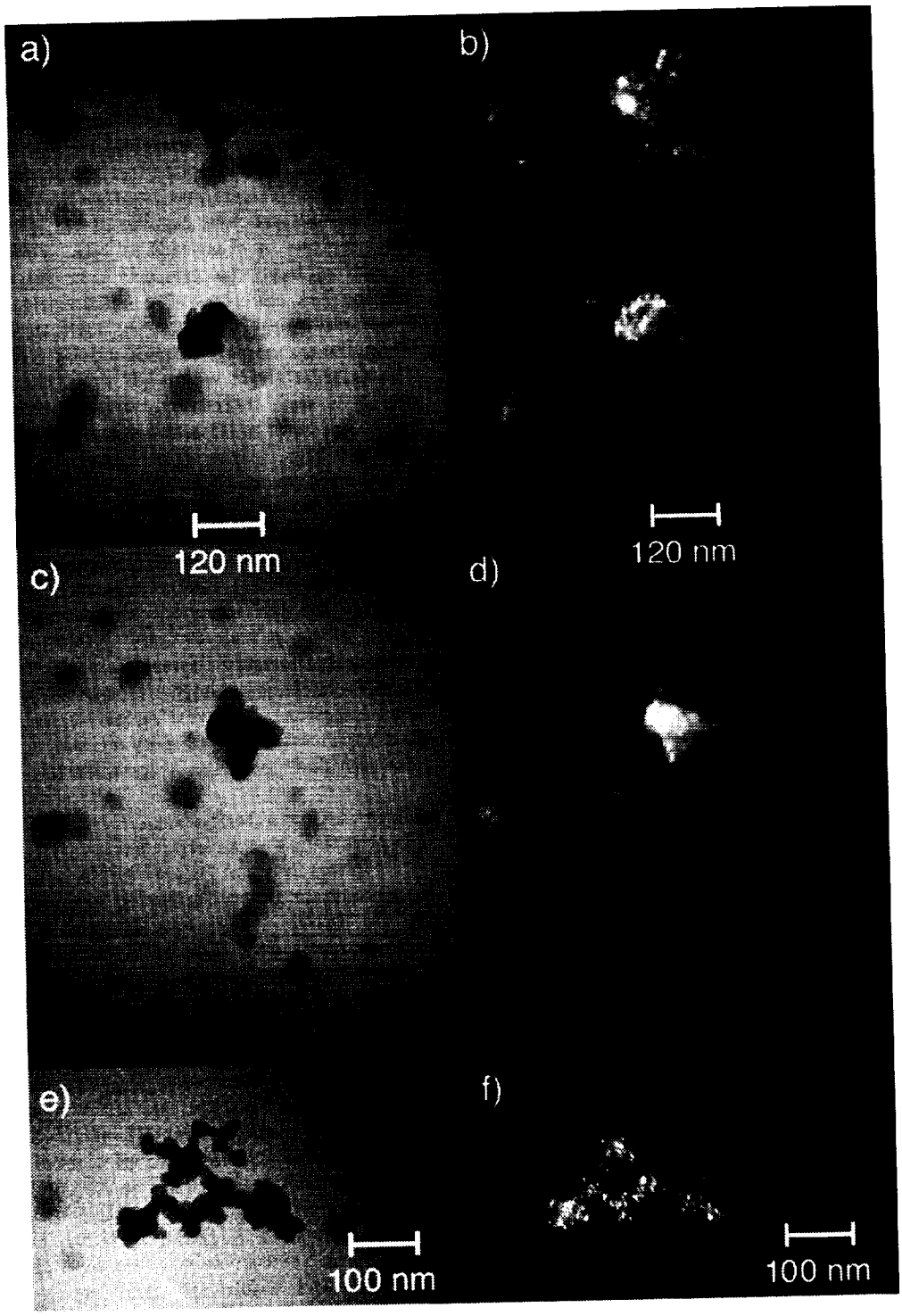

Figure 2.—Bright field TEM images, (a) and (c) of material sampled within the "transformation" region (indicated by the arrow in Fig. 1(a). The corresponding dark field TEM images are shown in (b) and (d). For comparison, Figs. 2(e) and 2(f) are matching bright and dark field TEM images of a typical soot aggregate such as may be found within the annular region of the diffusion flame.

and is consistent with rapid coalescence of pyrolysis products (PAHs) prior to significant carbonization [25]. The small size of several of the globules is also consistent with rapid material coalescence prior to significant aggregation to produce the familiar chain-like soot aggregates [5]. While many of the translucent globules appear as near spherical blobs, some appear to consist of individual subunits which are highly merged together. Thus, partial aggregation processes begin in this region prior to significant carbonization of the precursor particles. The diffuse halo surrounding some of the translucent globules also suggests an amorphous unstructured solid.

The noncrystalline nature of the tar-like appearing substance is confirmed by the dark field TEM micrographs shown in Figs. 2(b) and 2(d). The bright points in the dark field TEM images of Fig. 2(b) and 2(d) are interpreted as crystallites appropriately oriented to diffract a portion of the electron beam into the viewing angle [26]. Diffraction from ordered carbon layer planes indicates carbonization of these precursor particles has occurred with the chemical/ physical structure no longer resembling a "clump" of condensed hydrocarbons [27] but rather a disorganized solid [26]. Far less crystallinity of the globular tar-like appearing particles is revealed by their lower intensity (fewer "bright points" or crystallites) as compared to the central objects in Figs. 2(b) and 2(d) (which are the opaque objects in the bright field TEM images of Figs. 2(a) and 2(c)) and also in comparison to the dark field TEM image of a "normal" appearing soot aggregate shown in Fig. 2(f). While the range of opacities seen in the bright field TEM images is partially due to the varying thicknesses of the particles, it is also due to the varying structure (composition) of material of the particles. This is confirmed by the varying degrees of crystallinity observed for the tar-like globules within the dark field TEM images of Figs. 2(b) and 2(d). The wide variation in the crystallinity of the material within this region of the flame is also consistent with the optical measurements which show that significant fluorescence and incandescence arises from within this region as shown in Figs. 1(a) and 1(d).

Relationship to Photophysical Properties and Chemical Composition

The changes in the photophysical properties reflect the chemical and physical transformation in material properties occuring between predominately molecular material (condensed or gaseous) and solid carbonaceous soot. This transformation occurs in all flames producing soot.

Similar observations of rapid coalescence of pyrolysis fragments has been observed in flow reactor and shock tube studies of soot formation. The lack of geometrical definition and rather transparent appearance of some of the sampled material shown in Figs 2(a) and 2(c) is similar to previous TEM investigations of pyrolyzing benzene in a flow tube reactor at early residence times [28]. Similarly, in this diffusion flame, the fuel-rich side closely resembles a pyrolytic system with the flame front presenting an oxygen barrier [29]. The rapid rise of scattered light intensity concurrent with increasing ultraviolet absorption in the abscence of infrared absorption in shock tube experiments suggests a rapid coalescence of fuel pyrolysis products prior to significant carbonization as is observed here [30].

Chemical characterization of material sampled from within the pyrolysis region of premixed flames has identified significant amounts of aliphatic compounds [22]. Recent electron spectrocopy chemical analysis (ESCA) analysis of material sampled from within the pyrolysis regions of benzene and methane diffusion flames has likewise found significant amounts of aliphatic compounds within the material [31]. Most significantly, the structural changes observed via TEM are also consistent with the rapid chemical change observed by via laser microprobe mass analysis (LMMA) [5]. At 30 mm HAB, the hydrogen mole fraction of soot precursor material sampled from this region begins a rapid decrease from 0.36 towards 0.15, a value typical of mature soot.

Conclusions

Simultaneous LIF-LII images are valuable for visualizing both fuel pyrolysis and soot containing regions within diffusion flames. The LIF and LII signals may be distinguished either by the excitation wavelength dependence or the temporal decay following the laser pulse. Along flow trajectories proceeding from the fuel pyrolysis to soot containing regions a fundamental change in the material properties necessarily occurs. TEM observations of thermophoretically sampled material from the boundary region juxtaposed between the fuel pyrolysis and soot containing regions, reveal globular material with decreased density and markedly less crystallinity compared to normal soot aggregates. The appearance of the material in the TEM microscopy is consistent with the rapid coalescence of pyrolytic material prior to significant carbonization. Moreover, the beginning tranformation in the material properties observed via TEM supports observed changes in the photophysical properties of the soot precuror material in the transmutation towards solid carbonaceous soot.

Acknowledgements

Support under NASA contract NAS3-27186 for this work is acknowledged. The author extends special thanks to Mr. David Hull of NASA-LeRC for performing the TEM measurements and for very helpful discussions regarding TEM.

References

1. Wersborg, B.L., Fox, L.K. and Howard, J.B., Combust. and Flame 24:1 (1975).
2. Howard, J.B., *The Twenty-Third Symposium (International) on Combustion*, The Combustion Insititute, Pittsburgh, p. 1107-1127, 1990.
3. Miller, J.M., *Twenty-Third Symposium International) on Combustion*, The Combustion Insititute, Pittsburgh, 1980, p. 91.
4. McKinnon, J.T. and Howard, J.B., *Twenty-Fourth Symposium (International) on Combustion*, The Combustion Institute, Pittsburgh, 1992, p. 965.

5. Dobbins, R.A., Fletcher, R.A. and Lu, W., Combust. and Flame 100:301 (1995).
6. Vander Wal, R.L., Choi, M.Y. and Jensen, K.A. (Combust. and Flame, submitted).
7. Dobbins, R.A., and Subramaniasivam, H., (1994). *Soot precursor particles in flames. Soot Formation in Combustion*, (H. Bockhorn ed.), Springer Verlag, Berlin Heidelberg, 1994, p. 290.
8. Santoro, R.J., Semerjian, H.G., and Dobbins, R.A. Combust. and Flame 51:203 (1983).
9. Bengtsson, P.-E. and Alden, M., Combust. and Flame, 80:322 (1990).
10. Beretta, F., D'Alessio, A.D., D'Orsi, A., and Minutolo, P., Combust. Sci. and Technol., 85:455 (1992).
11. Letokhov, V. S., *Nonlinear Laser Chemistry: IRMPD*. Bristol, New York (1985).
12. Gomez, A., Littman, M.G. and Glassman, I., Combust. and Flame, 70:225 (1987).
13. Melton, L.A., Appl. Opt. 23:2201 (1984).
14. Dasch, C.J., Appl. Opt. 23:2209 (1984).
15. Hofeldt, D.L., SAE TP–930079 (Society of Automotive Engineers, Warrendale, PA 1993).
16. Eckbreth, A.C., *Laser Diagnostics for Combustion Temperature and Species*, Abacus Press, Cambridge, MA, 1988, p.301.
17. Vander Wal, R.L. and Weiland, K.J., J. Appl. Phys. B59:445 (1994).
18. Quay, V., Lee, T.-W., Ni, T. and Santoro, R.J., Combust. and Flame, 97:384 (1994).
19. Vander Wal, R. L. (Appl. Optics, submitted).
20. R.J. Santoro, T.T. Yeh, J.H. Horvath, and H.G. Semerjian, Combust. Sci. and Technol. 53:89 (1987).
21. Harris, S.J. and Weiner, A.M., *Twentieth Symposium (International) on Combustion*, The Combustion Institute, Pittsburgh, 1984, p. 969.
22. Ciajolo, A., D'Anna, A., Barbella, R. and Tregrossi, A., *Twenty-Fifth Symposium (International) on Combustion*, The Combustion Insititute, Pittsburgh, 1994, p. 679.
23. Turro, N.J., *Modern Molecular Photochemistry*, The Benjamin/Cummings Publishing Co., Menlo Park, 1978.
24. Parker, S. P. (1988). *The Solid State Physics Source Book*. McGraw Hill Book Co., New York, 1988, p. 95.
25. Jinno, H., Fukatani, S. and Takaya, A., *Sixteenth Symposium (International) on Combustion*, The Combustion Institute, Pittsburgh, 1976, p. 709.
26. Oberlin, A., Carbon 22:521 (1984).
27. Abrahamson, J., Nature 266:323 (1977).
28. Lahaye, J., *Physical aspects of nucleation and growth of soot particles in Particulate Carbon Formation During Combustion*, (D. C. Siegla and G. W. Smith eds.), Plenum Press, New York 1981, p. 143.
29. Gaydon, A.G. and Wolfhard, H.G., *Flames, Their structure, radiation and temperature*, Chapman and Hall, London, 4th ed., 1979.
30. Rawlins, W.T., Cowles, L.M. and Krech, R.H., *Twentieth Symposium (International) OnCombustion*, The Combustion Institute, Pittsburgh, 1984, p. 879.
31. Saito, K., Gordon, A.S., Williams, F.A. and Stickle, W.F., Combust. Sci. and Technol. 80:103 (1991).

REPORT DOCUMENTATION PAGE

Form Approved
OMB No. 0704-0188

1. AGENCY USE ONLY (*Leave blank*)	2. REPORT DATE	3. REPORT TYPE AND DATES COVERED
	May 1996	Final Contractor Report

4. TITLE AND SUBTITLE

Soot Precursor Material: Spatial Location via Simultaneous LIF-LII Imaging and Characterization via TEM

5. FUNDING NUMBERS

WU–963–70–0E
C–NAS3–27186

6. AUTHOR(S)

Randall L. Vander Wal

7. PERFORMING ORGANIZATION NAME(S) AND ADDRESS(ES)

NYMA, Inc.
2001 Aerospace Parkway
Brook Park, Ohio 44142

8. PERFORMING ORGANIZATION REPORT NUMBER

E–10188

9. SPONSORING/MONITORING AGENCY NAME(S) AND ADDRESS(ES)

National Aeronautics and Space Administration
Lewis Research Center
Cleveland, Ohio 44135–3191

10. SPONSORING/MONITORING AGENCY REPORT NUMBER

NASA CR–198470

11. SUPPLEMENTARY NOTES

Prepared for the Central States Section Meeting sponsored by The Combustion Institute, St. Louis, Missouri, May 5–7, 1996. Project Manager, Howard D. Ross, Space Experiments Division, NASA Lewis Research Center, organization code 6711, (216) 433–2562.

12a. DISTRIBUTION/AVAILABILITY STATEMENT

Unclassified - Unlimited
Subject Category 23

This publication is available from the NASA Center for AeroSpace Information, (301) 621–0390.

12b. DISTRIBUTION CODE

13. ABSTRACT ***(Maximum 200 words)***

The chemical and physical transformation between gaseous fuel pyrolysis products and solid carbonaceous soot represents a critical step in soot formation. In this paper, simultaneous two-dimensional LIF-LII images identify the spatial location where the earliest identifiable chemical and physical transformation of material towards solid carbonaceous soot occurs along the axial streamline in a normal diffusion flame. The identification of the individual LIF and LII signals is achieved by examining both the excitation wavelength dependence and characteristic temporal decay of each signal. Spatially precise thermophoretic sampling measurements are guided by the LIF-LII images with characterization of the sampled material accomplished via both bright and dark field TEM. Both bright and dark field TEM measurements support the observed changes in photophysical properties which account for conversion of fluorescence to incandescence as fuel pyrolysis products evolve towards solid carbonaceous soot.

14. SUBJECT TERMS

Soot precursor; Laser-induced fluorescence (LIF); Laser-Induced Incandescence (LII); Transmission Electron microscopy (TEM); Polycylic aromatic hydrocarbons

15. NUMBER OF PAGES

8

16. PRICE CODE

A02

17. SECURITY CLASSIFICATION OF REPORT	18. SECURITY CLASSIFICATION OF THIS PAGE	19. SECURITY CLASSIFICATION OF ABSTRACT	20. LIMITATION OF ABSTRACT
Unclassified	Unclassified	Unclassified	

National Aeronautics and
Space Administration

Lewis Research Center
21000 Brookpark Rd.
Cleveland, OH 44135-3191